AN APPROXIMATE ESTIMATION OF VELOCITY PROFILES AND TURBULENCE FACTOR MODELS FOR AIR-FLOWS ALONG THE EXTERIOR OF TEFC INDUCTION MOTORS

by

Dardan O. KLIMENTA[a,b*] and Antti HANNUKAINEN[a]

[a] Department of Mathematics and Systems Analysis, Aalto University, Aalto, Finland
[b] Faculty of Technical Sciences, University of Pristina in Kosovska Mitrovica, Kosovska Mitrovica, Serbia

Original scientific paper
https://doi.org/10.2298/TSCI150626090K

Compared to a number of other existing correlations for heat transfer, the empirical correlations for forced convection from a short horizontal cylinder in axial air-flows usually do not involve the effects of changes in air-flow velocity and/or air-flow turbulence. Therefore, a common analysis of the heat transfer by using only one energy balance equation for entire outer surface of a solid is considered insufficient for induction motor applications because it fails to include aforementioned effects. This paper presents a novel, empirically-based methodology to estimate approximately the values of air-flow velocities and turbulence factors, that is, velocity profiles and turbulence factor models for stationary horizontal cylinders with and without fins (frame and two end-shields) in axial air-flows. These velocity profiles and turbulence factor models can then be used in analytical modelling of steady-state heat transfer from the exterior of totally enclosed fan-cooled induction motors.

Key words: *air-flow velocity profile, empirical correlation, steady-state heat transfer, TEFC induction motor, turbulence factor model*

Introduction

In order to precisely apply an analytical model for steady-state heat transfer to any totally enclosed fan-cooled (TEFC) induction motor it is necessary to know the following: (1) two different air-flow velocities, one for the beginning and another for the end of the cooling channels; and (2) three different turbulence factor models, two particular models for the flat and cylindrical outer surfaces of the end-shields and one common for the cooling fins and the inter-fin surfaces. The introduction of these profiles and models facilitates estimation of the air-flow velocities and the turbulence factors for various TEFC induction motors.

The air-flow velocities at the beginning and at the end of the cooling channels of a TEFC induction motor are necessary to calculate the appropriate values of the Reynolds number. The Reynolds numbers are then used to calculate the average Nusselt numbers (by means of empirical correlations) and corresponding heat transfer coefficients due to forced convection (from end-shields, cooling fins, and inter-fin surfaces). However, the dependence of heat transfer coefficients for the cooling fins and the inter-fin surfaces on longitudinal distance from the fan cowl and corresponding temperature distribution (along the frame) can not be determined

* Corresponding author, e-mail: dardan.klimenta@aalto.fi; dardan.klimenta@pr.ac.rs

solely on the basis of the air-flow velocity profile [1]. This can be solved by introducing the dependence of the turbulence factor, $K_{\xi,y}$, on the longitudinal distance, y, in the form $K_{\xi,y} = K_{\xi,y}(y)$, which will be known as the turbulence factor model.

According to the Heiles [2], the turbulence factor, $K_{\xi,y}$, was introduced in the thermal analysis of the electrical machines based on the studies conducted by Rietschel in 1914 and Schutte in 1937. Moreover, according to them, the turbulence factor, $K_{\xi,y}$, is constant, does not depend on the air-flow velocity and typically has a value between 1.7 and 1.9. In 1965 Kovalev *et al.* [1] reported that for the frame of the motor with a shaft height of 180 mm, the degree of air-flow turbulence, ξ, decreases with the increase of the longitudinal distance from the fan cowl. The turbulence factor, $K_{\xi,y}$, should be distinguished from the degree of air-flow turbulence, ξ. Practically, the turbulence factor, $K_{\xi,y}$, represents the ratio between two values of the same heat transfer coefficient due to forced convection, $h_{ci}(\xi_1)$ and $h_{ci}(\xi_2)$, where the first corresponds to the degree of air-flow turbulence greater than zero ($\xi_1 > 0$) and the second to the degree of air-flow turbulence equal or close to zero ($\xi_2 = 0$ or $\xi_2 \approx 0$).

This paper proposes a set of new correlations for the air-flow velocity profiles and the turbulence factor models. The velocity profile is assumed to be a biquadratic polynomial function of the longitudinal distance from the fan cowl similar to the one from [3], but with no terms of odd-degree. The coefficients of this polynomial will depend on air-flow velocity at the beginning of the cooling channels, number of poles, height of the shaft, rated power and angular velocity of the rotor. Air-flow velocity at the beginning of the cooling channels and peripheral velocity of the fan wheel have been correlated by the one-nth-power law. The effect of the fan wheel shape on the air-flow velocities at the beginning and at the end of the cooling channels of induction motors is neglected. Velocity profiles have been obtained on the basis of the published experimental data on more than eighteen different TEFC induction motors and finned frames. The turbulence factor models, based on the existing data on five different TEFC induction motors, are assumed to be *reduction functions* similar to the one from [4].

Air-flow velocity profiles

According to [3], Pohlhausen in 1921 solved the momentum integral equation for a velocity distribution/profile within a laminar boundary layer along a flat plate. The velocity profile satisfies a polynomial of fourth degree [3]. Substituting the boundary layer thickness by the frame/fin length L_5 [m] and ignoring the terms of odd-degree in the polynomial, it is reasonable to assume that the profile of air-flow velocity along the cooling channels $V_y = f(y)$ [ms^{-1}] can be expressed as:

$$V_y = C_1 V_0 \left[1 - \Theta_0 \left(\frac{y}{L_5} \right)^2 + 0.5\Theta_0 \left(\frac{y}{L_5} \right)^4 \right] \tag{1}$$

where C_1 and Θ_0 are unknown dimensionless coefficients, V_0 [ms^{-1}] – the air-flow velocity at the beginning of the cooling channels, and y [m] – the longitudinal distance from the fan cowl. The coefficients C_1 and Θ_0 are determined based on the published experimental data with relevance to this problem.

The length, L_5, and the longitudinal distance, y, are defined in fig. 1, where the exterior of a standard TEFC induction motor is also presented. The exterior of a standard TEFC induction motor in the direction of fan wheel from the drive side consists of the following elements: (A) drive pulley, (B) metal key between pulley and shaft, (C) drive shaft extension, (D) drive end-shield, (E) finned frame, (F) terminal box, (G) metal nameplate, (H) eyebolt, (I) motor

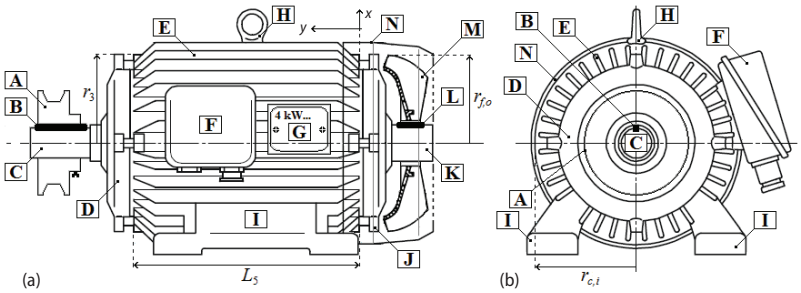

Figure 1. Standard TEFC induction motor; (a) side view, (b) view from the drive end of the shaft

mounting feet, (J) non-drive end-shield, (K) non-drive shaft extension, (L) metal key between fan wheel and shaft, (M) fan wheel, and (N) fan cowl. Element labels A-N correspond to the labelling within fig. 1. Furthermore, according to fig. 1, r_3 [m] is the frame radius under the fins, $r_{c,i}$ [m] is the inner radius of the fan cowl, and $r_{f,o}$ [m] is the outer radius of the fan wheel.

It is established that the coefficient C_1 depends only on the air-flow rate conditions. Each cooling channel along an actual frame may have a different air-flow rate. The difference in air-flow rate between different cooling channels is explained by means of the motor elements (bolt lugs and terminal box) which block the inlet and outlet zones of some cooling channels [5]. The value of the coefficient C_1 amounts to 1 or 2/3, which means that there is a negligible or significant effect of mechanical obstructions on the air-flow rate, respectively. As can be seen from fig. 4, the value $C_1 = 2/3$ corresponds approximately to the average air-flow rate along the frame cooling channels [5].

Moreover, it is assumed that the coefficient, Θ_0, depends on the ratio between the air-flow velocity at the beginning of the cooling channels V_0 [ms^{-1}] and the peripheral velocity of the fan wheel V_p [ms^{-1}], the shaft height H_{sh} [m], the angular velocity of the rotor Ω_m [rpm], the number of poles p, and the rated power P_n [kW]. This theory-based and empirically established dependence is described by the equation:

$$\Theta_0 = \left(\frac{V_0}{V_p} - H_{sh} \frac{\Omega_m}{C_2} \right) 2^{\left(2 - C_3 \frac{p}{8}\right)} \tag{2}$$

where C_2 [m·rpm] is a constant, and C_3 is an unknown dimensionless coefficient which depends on the number of poles, p, and the rated power, P_n. Fitting the available experimental data with the function (1) alone will give the values of C_2 and C_3.

Approximate equations for the ratio V_0/V_p for steady, fully developed, laminar, and turbulent flows of a Newtonian fluid through an annular gap between an equivalent non-drive end-shield and the fan cowl can be written as [6-9]:

$$\frac{V_0}{V_p} = \left(1 - \frac{r_3^2}{r_{c,i}^2} \right) \quad \text{for} \quad \text{Re} < 2320 \tag{3}$$

and

$$\frac{V_0}{V_p} = \left(1 - \frac{r_3}{r_{c,i}} \right)^{\frac{1}{n}} \quad \text{for} \quad \text{Re} \geq 2320 \tag{4}$$

respectively, where

$$n = [0.2525 - 0.0229 \cdot \log(\mathrm{Re})]^{-1} \tag{5}$$

is the exponent dependent on the Reynolds number $\mathrm{Re} = 2ur_{c,i}/\nu$, $u = 0.5V_p$ is the mean velocity in the case of laminar flow, and $u = 49V_p/60$ is the mean velocity in the case of turbulent flow. Equation (4) is an empirical equation known as the one-nth-power law/equation or the Nikuradse's equation for turbulent velocity profile in a pipe. According to the theory, the flow in a circular pipe is laminar if the Reynolds number is less than 2320 and turbulent, if it is greater than 4000. Between these two Reynolds numbers is a transitional zone where the flow can be laminar or turbulent or in the process of continuous switching between the two regimes. In the particular case of TEFC induction motors, it is also assumed that the eq. (4) can be a good approximation to the transition velocity profile. It is fairly safe because of the fact that the fan wheel and its cowl create the high turbulences at the beginning of the cooling channels [10-14]. The maximum of the velocity profile is at the outer radius of the fan wheel, $r_{f,o}$, and it amounts to the peripheral velocity of the fan wheel, V_p.

A number of studies have been published dealing with the profiles of air-flow velocity along the cooling channels of different TEFC induction motors, and a summary of them is presented in tab. 1. The values of the coefficients C_1, C_2, and C_3 are estimated based on these experimental data. Some of the V_0/V_p ratios in references cited in tab. 1 were reported as assumed, measured or averaged, but some of them were unspecified. In cases where it was possible the values of the ratio V_0/V_p are estimated by means of the one-7th-power equation and the definition of the peripheral velocity of the fan wheel:

$$V_p = \frac{2\pi r_{f,o}\Omega_m}{60} \tag{6}$$

where V_p is in [ms^{-1}] for $r_{f,o}$ in [m], and Ω_m in [rpm]. The one-7th-power equation is specifically used to avoid the calculation of the exponent n as well as the Reynolds number in the cases of absence of adequate geometric and heat transfer data in the literature.

Furthermore, in accordance with [4] for TEFC induction motors it can be stated that: (1) when the number of poles, p, increases the air-flow velocity along the cooling channels becomes smaller and smaller and (2) for motors having more than 4 poles it is acceptable to use only one value of the air-flow velocity along the cooling channels. Both these facts are fairly well implemented into the eq. (1).

Table 1. Summary of some published results relevant to the profiles of air-flow velocity along the cooling channels of TEFC induction motors

Ref.	Data for the test TEFC induction motors								Results[*d]		Remarks
	H_{sh}	p	P_n	Ω_m	r_3[*a]	$r_{c,i}$[*b]	$r_{f,o}$[*b]	L_5[*c]	V_0/V_p	$V_y = f(y)$	
	[mm]	[–]	[kW]	[rpm]	[mm]	[mm]	[mm]	[mm] or [p. u.]	[–]	[ms^{-1}] or [p. u.]	
[11]	80	2	1.1	2850	62.5	77	58	1 p.u.	0.75	fig. 4(a)-A	It was assumed that $V_0 \approx 0.75V_p$, $h_{c5} = f(V_0)$, and $h_{c6} = f(V_0)$.[*e]
[15]	100	4	1.5	1420	80.5	97.7	78	140	0.7	fig. 4(a)-C	It was assumed that $V_0 \approx 0.7V_p$, $h_{c5} = f(V_0)$, and $h_{c6} = f(V_0)$.[*e]

→

Table 1. (continuation)

Ref.	Data for the test TEFC induction motors								Results[*d]		Remarks
	H_{sh}	p	P_n	Ω_m	r_3[*a]	$r_{c,i}$[*b]	$r_{f,o}$[*b]	L_5[*c]	V_0/V_p	$V_y = f(y)$	
	[mm]	[–]	[kW]	[rpm]	[mm]	[mm]	[mm]	[mm] or [p. u.]	[–]	[ms^{-1}] or [p. u.]	
[4]	100	2	3	2870	78	96	76	160	n/a	fig. 4(a)-E	V_0 and V_y were expressed in p. u. and V_y was measured along the frame.
[4]	100	4	3	1430	78	96	76	160	n/a	fig. 4(a)-G	V_0 and V_y were expressed in p. u. and V_y was measured along the frame.
[16-18]	112	4	4	1435	88.5	108	85	1 p.u.	0.783	fig. 4(b)-A	It was found that V_0/V_p amounts between 0.043--0.783 for different blocked and unblocked channels.
[10]	112	4	4	1435	88.5	108	85	1 p.u.	0.478	fig. 4(b)-C and fig. 4(e)-A	Changes in air-flow velocities along the channels were averaged. The results are significantly different than the results obtained by other researchers for the similar motors.
[19]	112	4	4	1435	88.5	108	85	1 p.u.	n/a	fig. 4(b)-E	It was found that the average air-flow velocity along the frame amounts to $V_y = 5$ ms^{-1}.
[5]	112	4	4	1387.3	97.5	108	85	175	0.672	fig. 4(b)-F	Air-flow velocity along one of the unblocked channels was recorded.
[20]	112	4	4	≈1500	88.5	108	85	1 p.u.	0.562	fig. 4(c)-A	Air-flow velocity along the frame was measured at different supply frequencies f and motor line currents. Data on Ω_m = 1500, 1200, 900, 600, and 300 rpm correspond to f = 50, 40, 30, 20, and 10 Hz at a line current of 4.6 A, respectively.
	112	4	4	≈1200	88.5	108	85	1 p.u.	0.506	fig. 4(c)-C	
	112	4	4	≈900	88.5	108	85	1 p.u.	0.549	fig. 4(c)-E	
	112	4	4	≈600	88.5	108	85	1 p.u.	0.487	fig. 4(c)-G	
	112	4	4	≈300	88.5	108	85	1 p.u.	0.449	fig. 4(c)-I	
[14]	132	4	7.5	1500	104	127.5	100	1 p.u.	0.719	fig. 4(d)-A	Ω_m was adjusted from 300 up to 1500 rpm by controlling the armature voltage of a DC auxiliary motor.
	132	4	7.5	1200	104	127.5	100	1 p.u.	0.816	fig. 4(d)-C	
	132	4	7.5	900	104	127.5	100	1 p.u.	0.764	fig. 4(d)-E	
	132	4	7.5	600	104	127.5	100	1 p.u.	0.748	fig. 4(d)-G	
	132	4	7.5	300	104	127.5	100	1 p.u.	0.716	fig. 4(d)-I	
[10]	132	4	7.5	1450	104	127.5	100	1 p.u.	0.402	fig. 4(e)-C	The same remark as the one in the 6th row of this table.
[21]	132	4	9.2	n/a	104	127.5	100	1 p.u.	n/a	fig. 4(f)-A	V_0 at 80% of rated load was measured along the frame. Ω_m corresponded approx. to 2100 rpm.
[22]	132	4	9.2	n/a	104	127.5	100	1 p.u.	n/a	fig. 4(f)-B	

→

Table 1. (continuation)

Ref.	Data for the test TEFC induction motors								Results[*d]		Remarks
	H_{sh}	p	P_n	Ω_m	r_3[*a]	$r_{c,i}$[*b]	$r_{f,o}$[*b]	L_5[*c]	V_0/V_p	$V_y = f(y)$	
	[mm]	[–]	[kW]	[rpm]	[mm]	[mm]	[mm]	[mm] or [p. u.]	[–]	[ms^{-1}] or [p. u.]	
[12]	134/142	n/a	5.5	1800	111	134	67.5	250	0.739	fig. 4(g)-A	2 non-standard frames identical to the frames from [13] were analyzed under artificial ventilation. The frames were with: (1) N_{FE} = 36 and H_{FE} = = 23 mm and (2) N_{FE} = 48 and H_{FE} = 23 mm. Small differences were found. The tests corresponded approximately to p = 6.[*f]
	134/142	n/a	5.5	1500	111	134	67.5	250	0.745	fig. 4(g)-C	
	134/142	n/a	5.5	1200	111	134	67.5	250	0.719	fig. 4(g)-E	
	134/142	n/a	5.5	900	111	134	76	250	0.768	fig. 4(g)-G	
	134/142	n/a	5.5	600	111	134	76	250	0.733	fig. 4(g)-I	
	134/142	n/a	5.5	300	111	134	76	250	0.775	fig. 4(g)-K	
[13]	134/142	n/a	7.5	1800	111	134	100	250	0.739	fig. 4(h)-A	Four non-standard frames were analyzed under artificial ventilation. The frames were with: (1) N_{FE} = 48 and H_{FE} = = 31 mm, (2) N_{FE} = 48 and H_{FE} = 23 mm, (3) N_{FE} = 36 and H_{FE} = = 31 mm, and (4) N_{FE} = 36 and H_{FE} = 23 mm. Small differences were found. The tests corresponded approx. to p = 6.[*f]
	134/142	n/a	7.5	1500	111	134	100	250	0.801	fig. 4(h)-C	
	134/142	n/a	7.5	1200	111	134	100	250	0.739	fig. 4(h)-E	
	134/142	n/a	7.5	900	111	134	100	250	0.767	fig. 4(h)-G	
	134/142	n/a	7.5	600	111	134	100	250	0.759	fig. 4(h)-I	
	134/142	n/a	7.5	300	111	134	100	250	0.750	fig. 4(h)-K	
[10]	160	4	15	1435	125	153.5	120	1 p.u.	0.401	fig. 4(e)-E	The same remark as the one in the 6th row of this table.
[1]	180	n/a	n/a	n/a	115	175	n/a	450	n/a	fig. 4(f)-D	Air-flow velocity along the frame was averaged. V_0 and V_p were expressed in p.u.. p = 6, P_n=15 kW and $\Omega_m \approx$ 1000 rpm.[*g]
[14]	180	4	22	2100	142	172.5	141	1 p.u.	0.766	fig. 4(i)-A	Ω_m was adjusted by controlling the armature voltage of a DC auxiliary motor.
	180	4	22	1800	142	172.5	141	1 p.u.	0.674	fig. 4(i)-C	
[5]	180	6	15	917	149.8	172.5	140	370	0.837	fig. 4(i)-E	Air-flow velocity along one of the unblocked channels was recorded.
[5]	180	6	15	917	149.8	172.5	140	370	0.558	fig. 4(i)-G	Changes in air-flow velocities along the channels were averaged.
[10]	200	4	30	1460	157.5	191	155	1 p. u.	0.405	fig. 4(e)-G	The same remark as the one in the 6th row of this table.
[10]	250	4	55	1460	195	238.5	167.5	1 p. u.	0.531	fig. 4(e)-I	The same remark as the one in the 6th row of this table.
[23]	315	2	65	3600	252.5	298.5	200	1 p.u.	n/a	fig. 4(f)-F	Average air-flow velocity along the frame was modelled.

[*a] All values for the radius r_3 except those corresponding to [1, 5, 12, 13, 15] are estimated according to [24].

[*b] All values for the radii $r_{c,i}$ and $r_{f,o}$ except those corresponding to [1, 5, 15] are taken from [24], and they correspond to the TEFC induction motors which were analyzed in the aforemethioned references.

[*c] In most aforemethioned references, the longitudinal distance y was referred to the frame/fin length L_5, that is, y was expressed in [p. u.].

[*d] In order to estimate the unspecified values of the ratio V_0/V_p as well as the velocities V_p, V_0, and V_y in [ms^{-1}], the eqs. (4) and (6) for $n = 7$ and the radius $r_{f,o}$ are used.

[*e] Here h_{c5} [Wm^{-2}K^{-1}] is the heat transfer coefficient due to forced convection from the surfaces of the cooling fins, and h_{c6} [Wm^{-2}K^{-1}] is the heat transfer coefficient due to forced convection from the surfaces amongst the cooling fins.

[*f] Here N_{FE} is the number of the equivalent cooling fins, and H_{FE} [m] is the height of the equivalent cooling fins.

[*g] Values for p, P_n, and Ω_m are estimated according to [25].

Turbulence factor models

Based on the fact that the heat transfer coefficients due to forced convection from the cooling fins and the inter-fin surfaces simultaneously depend on the air-flow velocity profile and the degree of air-flow turbulence [1], the authors proposed the following *reduction function* for the turbulence factor model:

$$K_{\xi,y} = K_1 + (K_2 - K_1)\mathrm{e}^{-K_3 y} \tag{7}$$

where K_1 is a dimensionless coefficient representing the minimum value of the turbulence factor at very great distance from the fan cowl ($y \to \infty$), K_2 – the dimensionless coefficient representing the maximum value of the turbulence factor at zero distance from the fan cowl ($y = 0$), and K_3 [m^{-1}] – the coefficient which describes the reduction of the turbulence factor with the increase of the longitudinal distance from the fan cowl.

By means of an identical *reduction function* Di Gerlando and Vistoli [4] modelled the air-flow velocity profile along the same frames of two motors having the shaft height of 100 mm and different pole numbers. The experimental data on the degree of air-flow turbulence from [1] have been correlated with the *reduction function* (7) by setting $K_1 = 0.122$ and $K_2 = 0.4$ in accordance with [2] as well as $K_3 = 4.62$ in accordance with [4]. As can be seen from fig. 2, the generated solid curve coincides well with the experimental data represented by the cross markers. It is therefore evident that the reduction of the turbulence factor can be modelled by the eq. (7).

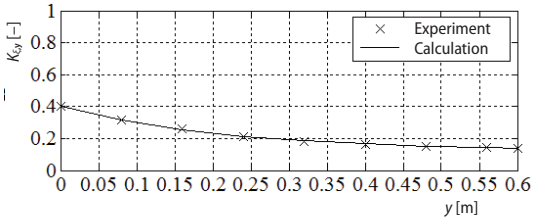

Figure 2. A comparison between the experimental data from [1] and the solid curve generated by means of the eq. (7) for $K_1 = 0.122$, $K_2 = 0.4$, and $K_3 = 4.62$

For the purposes of this study, the values of coefficients K_1 and K_2 are calculated by means of two auxiliary analytical algorithms. The algorithms are developed by assuming that a TEFC induction motor can be treated as a solid whose exterior can be described by a single energy balance equation. The flowchart, presented in fig. 3, describes simultaneously both algorithms. In this flowchart, all the assignments and conditions are common. The inputs, statements, functions and outputs which are outside of the round brackets are common for both algorithms or belong to the first one. The inputs, statements, functions and outputs inside the brackets, which are also preceded by the disjunctive *or*, only relate to the second algorithm.

The first/second algorithm comprises the energy balance equation in which the amount of heat dissipated (by forced convection and radiation) through both end-shields is expressed as

a multiple of the amount of heat dissipated through the drive/non-drive end-shield. According to fig. 3, the multiples associated with the first and second algorithms are designated with Δq_D and Δq_{ND}, respectively, where the subscripts *D* and *ND* refer to the drive and non-drive end-shield. Therefore, once the amounts of heat dissipated through the two end-shields are known, the energy balance equation can be solved without a number of empirical correlations. In the case of the first algorithm, for instance, correlations for forced convection from the flat and cylindrical outer surfaces of the non-drive end-shield [26-28] are not included in the iterative loop (in the 2nd set of statements). After the exit from the iterative loop, these correlations [26-28] are used for the calculation of the turbulence factors K_{2F} and K_{2C} corresponding to the flat and cylindrical outer surfaces of the non-drive end-shield, respectively. The subscripts *F* and *C*, respectively, denote the flat and cylindrical outer surfaces of the end-shields.

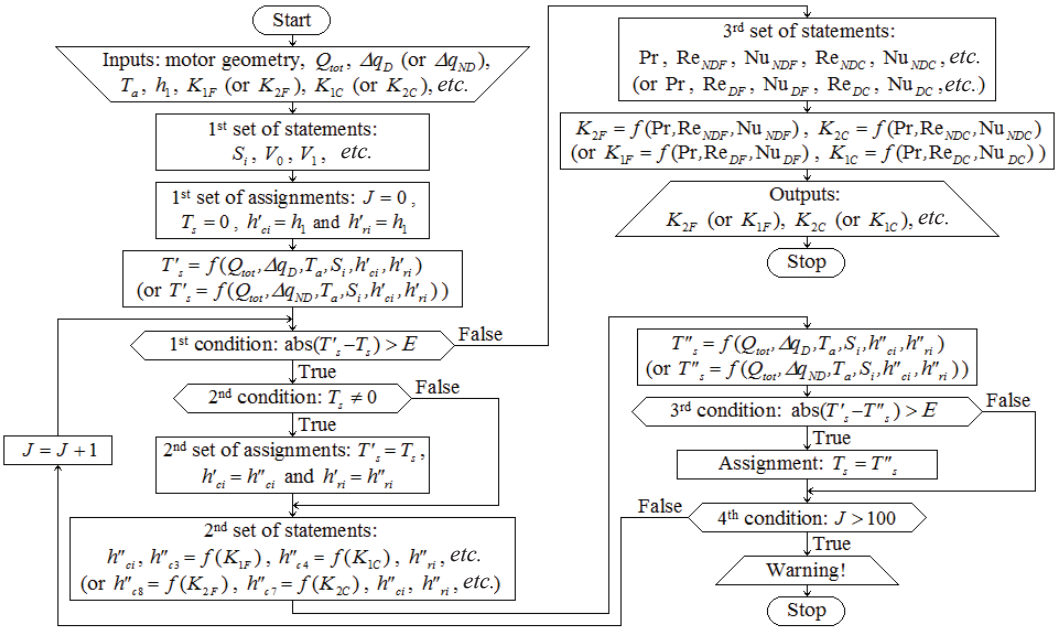

Figure 3. The flowchart illustrating the algorithms used for the calculation of K_1 and K_2

The parameters displayed in fig. 3 have the following meanings: Q_{tot} [W] is the total power loss, T_a [K] – the ambient air temperature, h_1 [Wm^{-2}K^{-1}] – an initial value for all heat transfer coefficients due to forced convection and radiation, K_{1F} [–] and K_{1C} [–] – are the turbulence factors corresponding to the flat and cylindrical outer surfaces of the drive end-shield, respectively, V_1 [ms^{-1}] – is the air-flow velocity at the end of the cooling channels, E [K] – the specified accuracy, J – the index of the current iteration, T_s [K] – the average temperature of the motor exterior, T'_s [K] and T''_s [K] – are the programme variables reserved for values of the temperature T_s, Pr is the Prandtl number, Re_{NDF}, Re_{NDC}, Re_{DF}, and Re_{DC} – corresponding Reynolds numbers, and Nu_{NDF}, Nu_{NDC}, Nu_{DF}, and Nu_{DC} – corresponding Nusselt numbers.

Moreover, S_1, S_2, ..., S_9, and S_{10} [m^2] are portions of the outer surface area of the motor. The coefficients h'_{c1}, h'_{c2}, … , h'_{c9} and h'_{c10} [Wm^{-2}K^{-1}] and h''_{c1}, h''_{c2}, … , h''_{c9} and h''_{c10} [Wm^{-2}K^{-1}] are the programme variables reserved for values of the heat transfer coefficients due to forced convection. The coefficients h'_{r1}, h'_{r2}, … , h'_{r9} and h'_{r10} [Wm^{-2}K^{-1}] and h''_{r1}, h''_{r2}, … , h''_{r9} and h''_{r10}

[$Wm^{-2}K^{-1}$] are the programme variables reserved for values of the heat transfer coefficients due to radiation. The subscripts $i = 3$ and $i = 8$ relate to the flat outer surfaces of the drive and non-drive end-shields, respectively. Also, $i = 4$ and $i = 7$ relate to the cylindrical outer surfaces of the drive and non-drive end-shields, respectively.

The values of the coefficient K_3 describing the reduction of the turbulence factor models are obtained by fitting curves through the values of K_1 and K_2 which were previously determined.

Results and discussions

Air-flow velocity profiles

Figure 4 illustrates the fitting procedure for determining the coefficients C_2 and C_3. The markers indicate measured air-flow velocities, expressed in [ms^{-1}] or [p. u.], and the curves except the solid curve with point markers corresponding to fig. 4(b)-E indicate calculated air-flow velocities.

Based on the comparisons, it is found: (1) that the coefficient C_2 amounts to 1500 m·rpm, and (2) that the values of the coefficient C_3 are: $C_3 = 3$ for $p \leq 4$ and $P_n \leq 15$ kW, $C_3 = 2$ for $p \leq 4$ and $P_n > 15$ kW, and $C_3 = 8/3$ for $p > 4$ and $\forall P_n$. This is in satisfactory agreement with most of the experimental data. The quantity of $P_n = 15$ kW that corresponds with the change in value of the coefficient C_3 also coincide with the fact that the TEFC induction motors of the rated powers up to 15 kW have an aluminum frame, while the motors of the rated powers above 15 kW have a cast iron one [16].

It is also important to note the large spread of values obtained in fig. 4. The cause for the large spread in data can be explained by the fact that the researchers utilized significantly different TEFC induction motors and frames, different loading conditions as well as different assumptions in their studies. Excluding the results reported in [10, 16-18], all other data are reliable and comparable. The best manner to show that is to discuss the results related to the four similar four-pole, 4 kW, 50 Hz TEFC induction motors from tab. 1, which are presented in fig. 4(b). Moreover, this motor is amongst the most commonly studied TEFC induction motors in the literature [5, 10, 16-20].

Amongst other details, it can be noticed from fig. 4(b) that the solid curve, fig. 4(b)-B, and the dashed curve, fig. 4(b)-D, fit well within the measured data which are labelled with the cross markers, fig. 4(b)-A. The solid curve passes over the maximum measured values of the air-flow velocity along the frame, while the dashed curve intersects almost ideally with the solid curve with point markers, fig. 4(b)-E, representing the average air-flow velocity along the frame. Compared to a curve that would pass through the square markers, fig. 4(b)-C, the dashed curve provided far better agreement with the cross markers, that is, with the measured data from [10, 16-18]. According to these references, the value of the average air-flow velocity along the frame is significantly lower than 5 m/s and amounts to approximately 4 m/s. Moreover, the dotted curve, fig. 4(b)-G, does not fit so well within the measured data from [5] which are labelled with the plus sign markers, fig. 4(b)-F. However, substituting the estimated value of the ratio $V_0/V_p = 0.717$ (which is calculated by using the eqs. (4) and (6) for $n = 7$) by the tabulated value $V_0/V_p = 0.672$ into the eq. (2), it would be possible to provide better agreement between the dotted curve and the plus sign markers.

From the same authors, such the differences were also obtained for four-pole TEFC induction motors of the rated powers of 7.5, 15, 30, and 55 kW [10, 16-18]. It can also be noticed in fig. 4(e). The reasons for this are the same as those previously described. The fact that there is an underestimation or overestimation of the average air-flow velocities along the frames of these motors can also be supported by data from the motor guides [29, 30]. By comparing

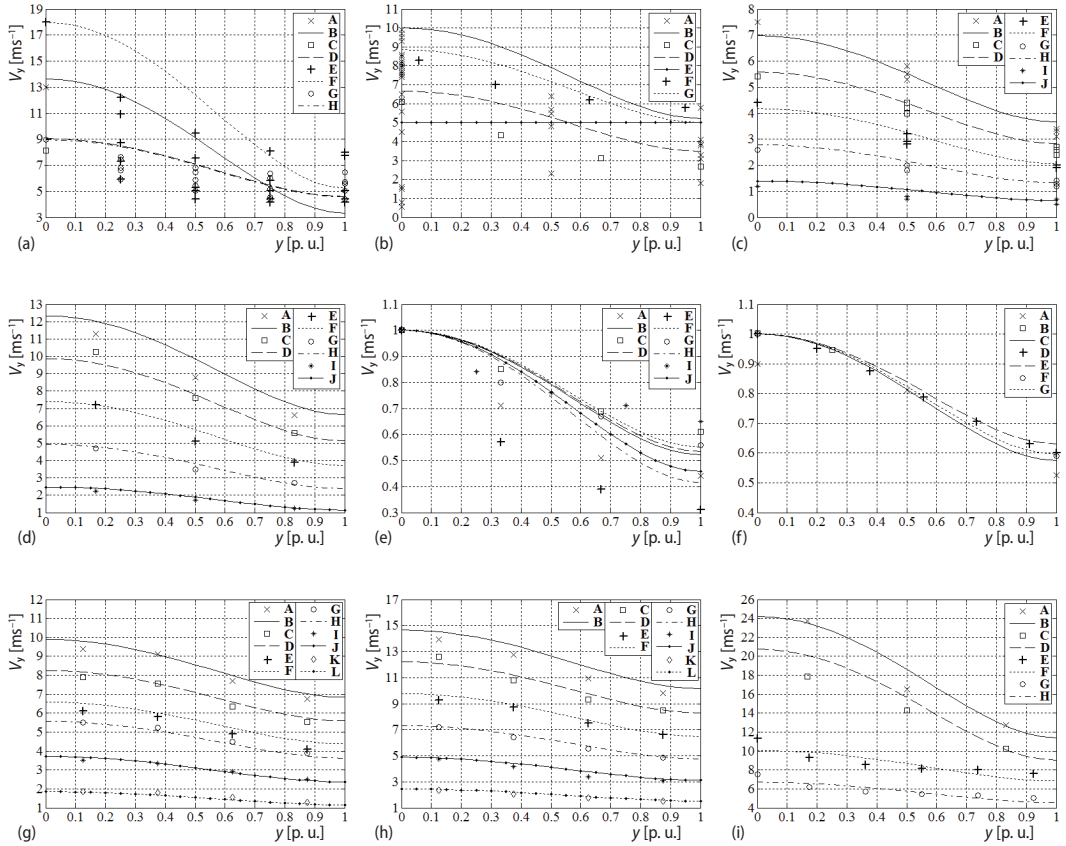

Figure 4. Comparisons of the results which are outlined in tab. 1 with the results generated by means of eq. (1) for: (a) $C_1 = 1$ and $C_3 = 3$ – for all curves, (b) $C_1 = 1$ and $C_3 = 3$ – for solid and dotted curves, $C_1 = 2/3$ and $C_3 = 3$ – for dashed curve, (c) $C_1 = 2/3$ and $C_3 = 3$ – for all curves, (d) $C_1 = 1$ and $C_3 = 3$ – for all curves, (e) $C_1 = 1$ and $C_3 = 3$ – for solid, dashed, and dotted curves, $C_1 = 1$ and $C_3 = 2$ – for dash-dot curve and solid curve with point markers, (f) $C_1 = 1$ and $C_3 = 3$ – for solid curve, $C_1 = 1$ and $C_3 = 8/3$ – for dashed curve, $C_1 = 1$ and $C_3 = 2$ – for dotted curve, (g) $C_1 = 1$ and $C_3 = 8/3$ – for all curves, (h) $C_1 = 1$ and $C_3 = 8/3$ – for all curves, and (i) $C_1 = 1$ and $C_3 = 2$ – for solid and dashed curves, $C_1 = 1$ and $C_3 = 8/3$ – for dotted curve, $C_1 = 2/3$ and $C_3 = 8/3$ – for dash-dot curve

the values of the air-flow velocity at the beginning of the cooling channels from [10, 16-18] and the corresponding minimum values from [29], it can be concluded that there are significant differences between these values. These differences amount to –12.8, –32.2, –9.7, –4, and +13.3% for motors of the rated powers of 4, 7.5, 15, 30, and 55 kW, respectively. If one excludes the underestimation (or overestimation) of the average air-flow velocities along the frames, then the following conclusion can be drawn: these motors were not designed in accordance with the standards. However, that was not the case with these motors. Therefore, the experimental results reported in [10, 16-18] could not be used in a better manner for this study.

Turbulence factor models

If it is assumed that the turbulence factors at zero distances from the fan cowls are the same for all the motors and that their values depend only on the longitudinal distance; then,

based on the experimental data related to the 4 and 15 kW motors from [5] and by means of two auxiliary analytical algorithms, which were previously presented in the section *Turbulence factor models*, the following equations are obtained:

$$K_{\xi,y} = 1 + (1.4163 - 1)\mathrm{e}^{-4.62y} \quad \text{– for flat outer surfaces of end-shields} \tag{8}$$

$$K_{\xi,y} = 1 + (1.6776 - 1)\mathrm{e}^{-13.087y} \quad \text{– for cylindrical outer surfaces of end-shields} \tag{9}$$

$$K_{\xi,y} = 1 + (1.8 - 1)\mathrm{e}^{-13.087y} \quad \text{– for fins and inter-fin surfaces} \tag{10}$$

The values of coefficients K_1, K_2, and K_3 defined in the aforementioned three equations are obtained in the following manner.

– For the motors having longer axial lengths, based on the results reported in [1], it is obvious that the degree of air-flow turbulence at the drive end approximately equals to zero. That is why the effect of turbulence on the heat transfer at the drive end of motors with longer axial lengths can be ignored and why the coefficient K_1 equals to 1 in all three equations.
– In [5] it is reported that the amounts of heat dissipated through the drive end-shield and the non-drive end-shield of the 15 kW motor at rated operation equal to 6 and 12 % of Q_{tot}, respectively. By introducing this experimental data into associated energy balance equation for the 15 kW motor exterior and assuming that $K_{1F} = K_{1C} \approx 1$ at a distance $y = L_5 = 0.37$ m, the authors found that K_2 amounts to $K_{2F} = 1.4163$ and $K_{2C} = 1.6776$ for the flat and cylindrical outer surfaces of the end-shields, respectively.
– According to [5], the portions of heat dissipated through the drive end-shield and the non-drive end-shield of the 4 kW motor at rated operation equal to 9 and 19 % of Q_{tot}, respectively. By substituting this data into associated energy balance equation for the 4 kW motor exterior and assuming that $K_2 = K_{2F} = 1.4163$ and $K_2 = K_{2C} = 1.6776$ (for the flat and cylindrical outer surfaces of the end-shields), the authors found that K_1 amounts to $K_{1F} = 1.2385$ and $K_{1C} = 1.0686$ for the flat and cylindrical outer surfaces of the end-shields, respectively.
– It is estimated that the models which fit well within the previously-calculated values of the turbulence factors for the flat and cylindrical outer surfaces of the end-shields have the exponents $K_3 = K_{3F} = 4.62$ and $K_3 = K_{3C} = 13.087$, respectively. Figure 5 depicts the models (8) and (9), that is, the dashed and dotted curves, together with corresponding calculated values of the turbulence factor (represented by the square and plus sign markers).
– The turbulence factor model (10) is derived from the model (9) by substitution of the calculated value of the coefficient $K_2 = 1.6776$ by the arithmetic mean of the two bounds of the range 1.7-1.9, which is reported in [2]. The model (9) is derived by using the correlations for turbulent forced convection from a cylinder in axial air-flows, which correspond to the degree of air-flow turbulence $\xi = 0.1\%$ [26-28]. Therefore, if the degree of air-

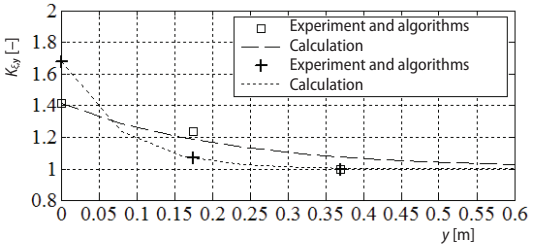

Figure 5. A comparison of the square markers calculated by using the experimental data from [5] and the auxiliary algorithms for the flat outer surfaces of the end-shields with the dashed curve generated by means of eq. (8) and a comparison of the plus sign markers calculated by using the experimental data from [5] and the auxiliary algorithms for the cylindrical outer surfaces of the end-shields with the dotted curve generated by means of eq. (9)

flow turbulence is equal to zero ($\xi = 0\%$), the model (10) can be used instead of (9) for the cylindrical outer surfaces of the end-shields, but in combination with the appropriate correlations for laminar forced convection.

Conclusion

The authors developed an empirically-based methodology for estimating air-flow velocity profiles and turbulence factor models along the frames of various TEFC induction motors. By using the velocity profiles and the turbulence factor models, it is possible now to express the energy balance on the exterior of any TEFC induction motor with just a single equation and to determine accurately the steady-state axial temperature distribution (along the cooling channels). Therefore, the methodology establishes a general framework for developing novel analytical models for steady-state thermal analysis of induction motors. The velocity profiles and turbulence factor models have been obtained on the basis of a representative sample of TEFC induction motors.

Acknowledgment

This research was conducted within the project 259873 funded by the Academy of Finland.

References

[1] Kovalev, E. B., *et al*., Heat Release in Channels between Frame-Ribbing of Enclosed Asynchronous Motors, *Elektrotekhnika, 36* (1965), 11, pp. 27-29
[2] Heiles, F., On the Appropriate Design and Arrangement of Cooling Fins (in German), *Elektrotechnik und Maschinenbau, 69* (1952), 14, pp. 323-331
[3] Chanson, H., *Applied Hydrodynamics: An Introduction*, CRC Press, Taylor & Francis Group, LLC, Leiden, The Netherlands, 2014, pp. 253-286
[4] Di Gerlando, A., Vistoli, I., Improved Thermal Modelling of Induction Motors for Design Purposes, *Proceedings*, IET 6th International Conference on Electrical Machines and Drives, No. 376, Oxford, UK, 1993, pp. 381-386
[5] Kylander, G., Thermal Modelling of Small Cage Induction Motors, Ph. D. thesis, School of Electrical and Computer Engineering, Chalmers University of Technology, Gothenburg, Sweden, 1995
[6] Hewitt, G. F., Hall-Taylor, N. S., *Annular Two-Phase Flow*, Pergamon Press, Oxford, UK, 1970
[7] Balachandran, P., *Engineering Fluid Mechanics*, PHI Learning Private Limited, New Delhi, India, 2011, pp. 232-275
[8] Webster, J. G., Eren, H., *Measurement, Instrumentation, and Sensors Handbook: Spatial, Mechanical, Thermal, and Radiation Measurement*, 2nd ed., CRC Press, Taylor & Francis Group, LLC, Boca Raton, Fla., USA, 2014, pp. 57.6-57.8
[9] Holland, F. A., Bragg, R., *Fluid Flow for Chemical Engineers*, 2nd ed., Butterworth-Heinemann, Oxford, UK, 1995, pp. 85-88
[10] Staton, D. A., Cavagnino, A., Convection Heat Transfer and Flow Calculations Suitable for Electric Machines Thermal Models, *IEEE Transactions on Industrial Electronics, 55* (2008), 10, pp. 3509-3516
[11] Romo, J. L., Adrian, M. B., Prediction of Internal Temperature in Three-Phase Induction Motors with Electronic Speed Control, *Electric Power Systems Research, 45* (1998), 2, pp. 91-99
[12] Valenzuela, M. A., Tapia, J. A., Heat Transfer and Thermal Design of Finned Frames for TEFC Variable Speed Motors, *Proceedings,* 32nd Annual Conference on IEEE Industrial Electronics – IECON 2006, Paris, 2006, pp. 4835-4840
[13] Valenzuela, M. A., Tapia, J. A., Heat Transfer and Thermal Design of Finned Frames for TEFC Variable-Speed Motors, *IEEE Transactions on Industrial Electronics, 55* (2008), 10, pp. 3500-3508
[14] Valenzuela, M. A., *et al*., Thermal Evaluation of TEFC Induction Motors Operating on Frequency-Controlled Variable-Speed Drives, *IEEE Transactions on Industry Applications, 40* (2004), 2, pp. 692-698
[15] Huai, Y., *et al*., Computational Analysis of Temperature Rise Phenomena in Electric Induction Motors, *Applied Thermal Engineering, 23* (2003), 7, pp. 779-795

[16] Boglietti, A., *et al*., Determination of Critical Parameters in Electrical Machine Thermal Models, *IEEE Transactions on Industry Applications, 44* (2008), 4, pp. 1150-1159
[17] Boglietti, A., *et al*., Thermal Aanalysis of TEFC Induction Motors, *Proceedings*, IEEE Industry Applications Conference – 38th IAS Annual Meeting, Salt Lake City, Ut., USA, 2003, Vol. 2, pp. 849-856
[18] Boglietti, A., *et al*., TEFC Induction Motors Thermal Models: A Parameter Sensitivity Analysis, *IEEE Transactions on Industry Applications, 41* (2005), 3, pp. 756-763
[19] Fernandez, X. M. L., *et al*., Thermal Analysis of an Induction Motor Fed by Unbalanced Power Supply Using a Combined Finite Element – Symmetrical Components Formulation, *Proceedings,* International Conference on Power System Technology – POWERCON '98, Beijing, 1998, Vol. 1, pp. 620-624
[20] Mendes, A. M. S., *et al*., Thermal Evaluation of TEFC Three-Phase Induction Motors under Different Supply Frequencies, *Proceedings,* 18th International Conference on Electrical Machines – ICEM 2008, Vilamoura, Portugal, 2008, ID 1069
[21] Valenzuela, M. A., *et al*., Effect of Protective Covers for TEFC Induction Motors Covered by Pulp, *Proceedings*, Annual Pulp and Paper Industry Technical Conference, Appleton, Wis., USA, 2006, pp. 1-7
[22] Valenzuela, M. A., *et al*., Thermal Derating of TEFC Induction Motors Coated or Partially Flooded by Spilled Pulp, *Proceedings*, Annual Pulp and Paper Industry Technical Conference, Victoria, B. C., Canada, 2004, pp. 8-14
[23] Moon, S.-H., *et al*., Thermal-Flow Analysis and Cooling Performance Enhancement of a Totally Enclosed Fan-Cooled Motor, *Proceedings*, International Conference on Electrical Machines and Systems – ICEMS 2013, Busan, Republic of Korea, 2013, pp. 2028-2030
[24] ***, KMMP, *Electric Motors & Components*, Kurt Maier Motor-Press GmbH, Kalefeld, Germany, 2014
[25] Koyasu, E., Ito, T., New Series Standard Induction Motor with Class E Insulation, *Fuji Electric Review, 10* (1964), 4, pp. 130-136
[26] Wiberg, R., Lior, N., Heat Transfer from a Cylinder in Axial Turbulent Flows, *International Journal of Heat and Mass Transfer, 48* (2005), 8, pp. 1505-1517
[27] Kobus, C. J., Shumway, G., An Experimental Investigation into Impinging Forced Convection Heat Transfer from Stationary Isothermal Circular Disks, *International Journal of Heat and Mass Transfer, 49* (2006), 1-2, pp. 411-414
[28] Kobus, C. J., Wedekind, G. L., An Experimental Investigation into Forced, Natural and Combined Forced and Natural Convective Heat Transfer from Stationary Isothermal Circular Disks, *International Journal of Heat and Mass Transfer, 38* (1995), 18, pp. 3329-3339
[29] ***, ABB LV Motors, GB 02-2005**,** *The Motor Guide – Basic Technical Information about Low Voltage Standard Motors*, 2nd ed., ABB, Finland, 2005, pp. 34-46
[30] ***, ABB Motors and Generators, 9AKK105285 EN 02-2014, *The Motor Guide – Basic Technical Information about Low Voltage Standard Motors*, 3rd ed., ABB, Finland, 2014, pp. 24-39, 65

Paper submitted: June 26, 2015
Paper revised: April 22, 2016
Paper accepted: April 22, 2016